Structural Engineering and Mechanics, Vol. 18, No. 5 (2004) 645-669
DOI: http://dx.doi.org/10.12989/sem.2004.18.5.645

Modeling of cyclic joint shear deformation contributions in RC beam-column connections to overall frame behavior

Myoungsu Shin†

Morehead State University, Department of Industrial and Engineering Technology, 309 Lloyd Cassity, Morehead, Kentucky, 40351, U.S.A.

James M. LaFave†

University of Illinois at Urbana-Champaign, Department of Civil and Environmental Engineering, 3108 Newmark Civil Engineering Laboratory, MC-250, 205 North Mathews Avenue, Urbana, Illinois, 61801, U.S.A.

(Received January 28, 2004, Accepted June 14, 2004)

Abstract. In seismic analysis of moment-resisting frames, beam-column connections are often modeled with rigid joint zones. However, it has been demonstrated that, in ductile reinforced concrete (RC) moment-resisting frames designed based on current codes (to say nothing of older non-ductile frames), the joint zones are in fact not rigid, but rather undergo significant shear deformations that contribute greatly to global drift. Therefore, the "rigid joint" assumption may result in misinterpretation of the global performance characteristics of frames and could consequently lead to miscalculation of strength and ductility demands on constituent frame members. The primary objective of this paper is to propose a rational method for estimating the hysteretic joint shear behavior of RC connections and for incorporating this behavior into frame analysis. The authors tested four RC edge beam-column-slab connection subassemblies subjected to earthquake-type lateral loading; hysteretic joint shear behavior is investigated based on these tests and other laboratory tests reported in the literature. An analytical scheme employing the modified compression field theory (MCFT) is developed to approximate joint shear stress vs. joint shear strain response. A connection model capable of explicitly considering hysteretic joint shear behavior is then formulated for nonlinear structural analysis. In the model, a joint is represented by rigid elements located along the joint edges and nonlinear rotational springs embedded in one of the four hinges linking adjacent rigid elements. The connection model is able to well represent the experimental hysteretic joint shear behavior and overall load-displacement response of connection subassemblies.

Key words: reinforced concrete; beam-column connection; joint shear deformation; bond slip; numerical modeling; frame analysis.

1. Introduction

In reinforced concrete moment-resisting frame (RCMRF) structures under severe ground motions, beam-column connections are subjected to moment reversals across the joint due to the adjacent

† Assistant Professor

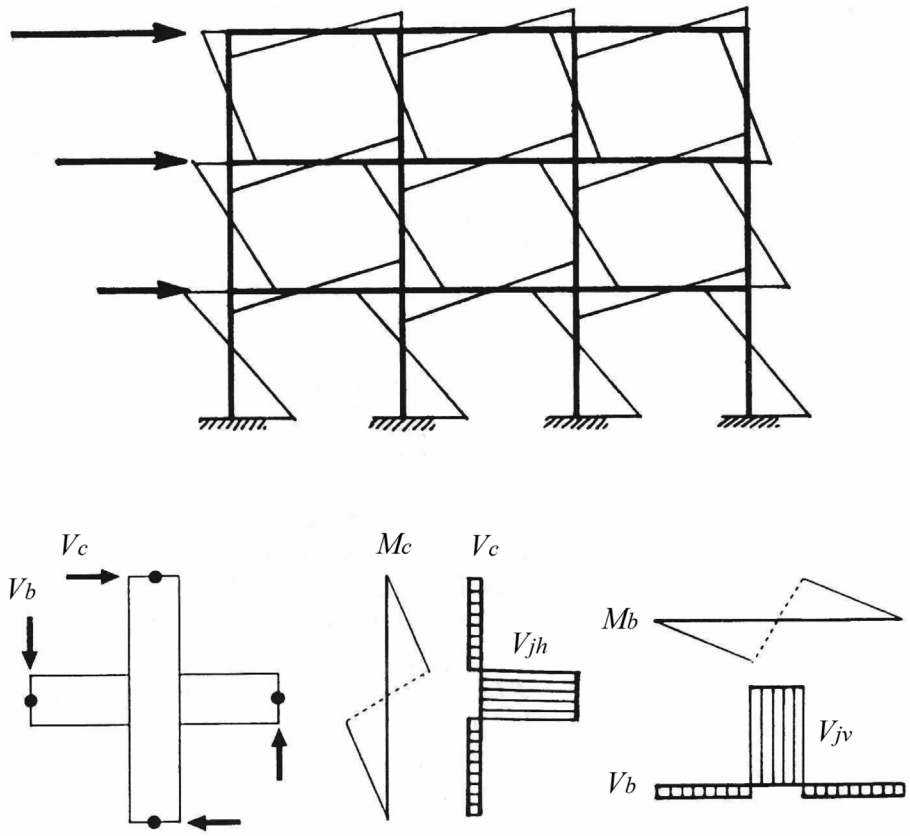

Fig. 1 A moment resisting frame subjected to lateral loading (adopted from CEB (1996))

beams and columns. As a result, the joint regions undergo significant horizontal (and vertical) shear forces whose magnitudes are much larger than those in the adjacent members (Fig. 1). Also, beam and column reinforcing bars passing through the joint are subjected to tension at one boundary of the joint and compression at the other because of the moment reversals. To sustain these forces, high bond stresses are required between the joint concrete and the longitudinal bars.

According to the capacity design philosophy, large displacement demands imposed on an RCMRF structure during severe ground motions can be endured with appropriately detailed plastic hinges in chosen members, which are typically the beams in frame structures. The well-detailed members must be equipped with sufficient ductility to permit an adequate global displacement capacity of the structure. Beam-column joints are not particularly suitable as primary energy dissipating sources because the behavior of joints is governed by shear and bond mechanisms, both of which typically exhibit poor hysteretic properties. Therefore, beam-column joints are usually designed with the intention that they should remain within their elastic range of behavior.

However, it has been demonstrated by laboratory tests and post-earthquake inspections that, in ductile RCMRF structures designed based on current codes (to say nothing of older non-ductile frames), joints may in fact undergo significant inelastic shear deformations. Moreover, both elastic and inelastic shear deformations of joints may contribute greatly to story drifts in frames.

Nevertheless, in seismic analyses of RCMRF structures, beam-column connections are often modeled with rigid joint zones (i.e., rigid member-end offsets in a centerline model), regardless of the joint details, while primary concern is focused on whether well-detailed beam plastic hinges can endure imposed displacement demands and whether other members can remain within their elastic ranges. Due to the "rigid joint" assumption, the contribution of joint shear deformation to overall frame displacement is neglected, and joint shear failure cannot be identified. This can result in misinterpretation of the global performance (stiffness, strength, and dynamic characteristics) of structures and could consequently lead to miscalculation of local strength and ductility demands on constituent members.

The primary objective of this paper is to propose a rational method for estimating the hysteretic joint shear behavior of RCMRF connections that can be incorporated into frame analysis. The focus is on ductile moment frames designed and detailed following modern seismic code requirements (rather than on older non-ductile frames with little or no joint shear reinforcement). The authors tested four RC edge beam-column-slab connection subassemblies subjected to simulated lateral loading; hysteretic joint shear behavior is investigated based on these tests and other laboratory tests reported in the literature. Then an analytical scheme employing the modified compression field theory (MCFT) is proposed to approximate joint shear stress vs. joint shear strain curves and is verified based on the experimental investigations. Finally, a connection model capable of explicitly considering hysteretic joint shear behavior is formulated using DRAIN-2DX (nonlinear structural analysis software); this connection model also takes into account fixed end rotations arising at beam/joint interfaces due to bond slip and yielding of longitudinal beam bars in the joint, as well as plastic hinge rotations at the ends of beams. Appropriate hysteretic models are adopted to represent these various nonlinear connection behaviors. The overall connection model is demonstrated by applying to RC beam-column connection subassemblies.

2. Previous joint modeling studies

Several researchers have creatively worked to model nonlinear hysteretic joint behavior in frames under lateral ground excitations, toward reproducing overall beam-column connection performance. These studies range from lumped empirical calibration methods to refined finite element analyses. An early generation work by Giberson (1969) proposed a simple beam model consisting of one perfectly elastic element and two nonlinear rotational springs attached at the ends of the elastic element (Fig. 2). Using this type of "one-component" model (e.g., Otani 1974, Anderson and Townsend 1977, Raffaelle and Wight 1992), all nonlinear deformations occurring at a beam-column connection were lumped at the moment vs. rotation response of the beam (and/or column) springs that were empirically calibrated for the particular connection. (A hysteresis relationship proposed by Takeda *et al.* (1970) was frequently used for representing the moment vs. rotation response.) This model is capable of implicitly including joint shear deformation contributions to overall story displacement, but it can produce inaccurate local strength and ductility demands, cannot identify local mechanisms such as joint shear failure, and generally lacks explicit treatment of joint shear behavior.

Krawinkler and Mohasseb (1987) pioneered introduction of a macro-element model capable of considering the effect of panel zones on the global behavior of steel moment-resisting frames (Fig. 3). Each panel zone consisted of two scissor-type rigid elements connected by a hinge, as well as a

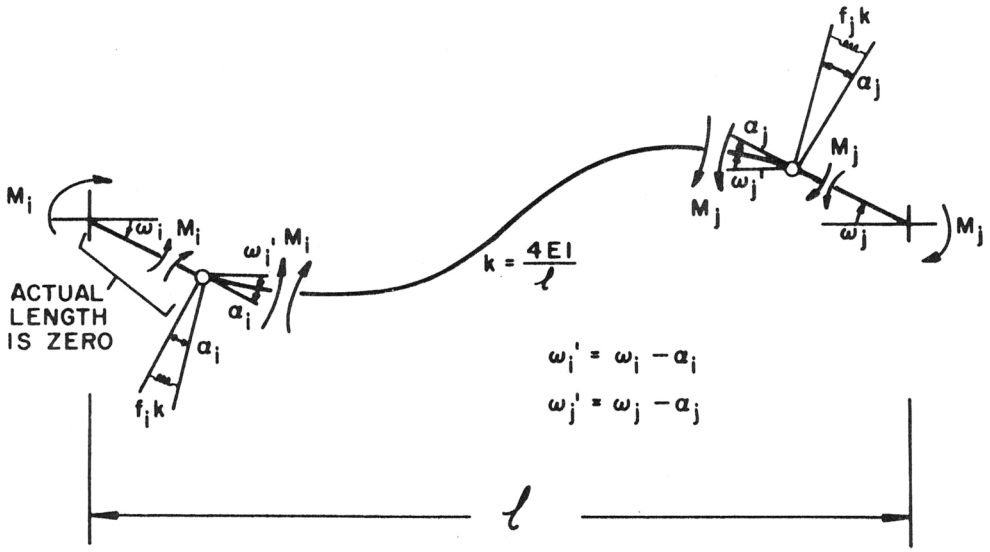

Fig. 2 One-component model of a nonlinear beam proposed by Giberson (1969)

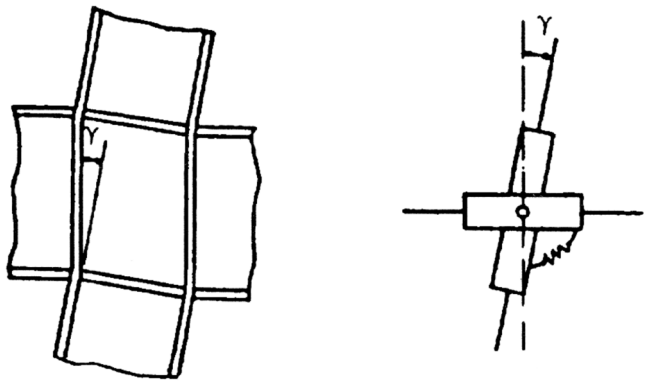

Fig. 3 Steel panel zone model proposed by Krawinkler and Mohasseb (1987)

nonlinear rotational spring that represented the shear force vs. shear deformation behavior of the panel zone. The moment at the rotational spring was approximately considered as the moment transferred from the beams to the column at the column faces. The lengths of the scissors were assumed equal to the beam and column depths. Later, Krawinkler (2001) developed a more accurate panel zone model with rigid boundaries. The shear force vs. shear deformation relation of steel panel zones was defined as tri-linear (with a plateau after reaching the joint shear strength), using simple equations for yield and ultimate points.

For RC connections, Alath and Kunnath (1995) presented a joint model using a rotational spring, similar to the Krawinkler and Mohasseb scissor model mentioned above. The panel moments were computed from the column and beam moments, assuming the joint core was under pure shear, but joint shear properties were empirically determined for each case. Biddah and Ghobarah (1999) modified the Alath and Kunnath scissor-type model by employing two nonlinear rotational springs

in series (Fig. 4) – one for joint shear deformations and the other for rotations due to bond slip of beam reinforcing bars near the joint region. The shear stress vs. shear deformation response of a

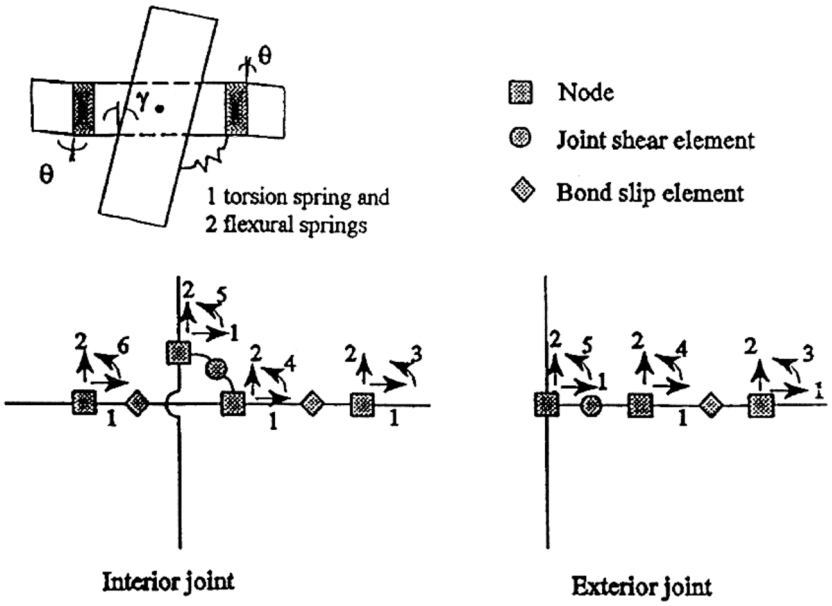

Fig. 4 RC joint model proposed by Biddah and Ghobarah (1999)

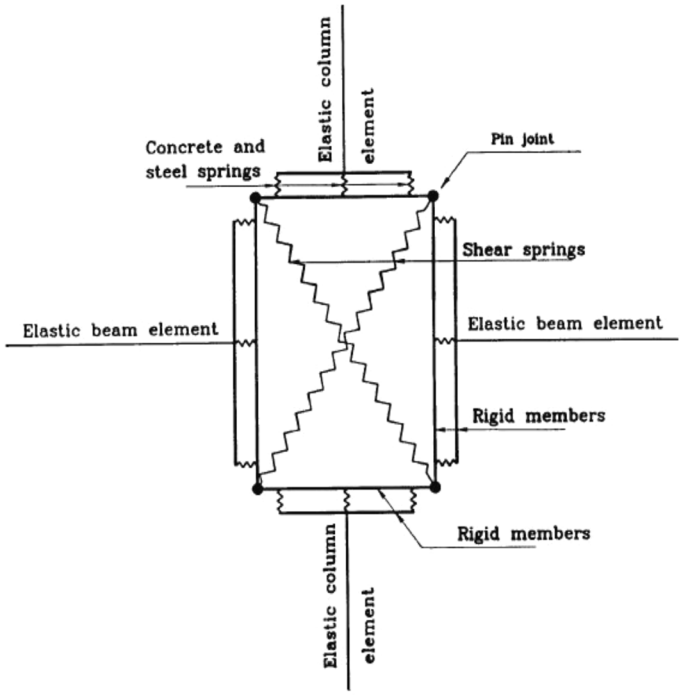

Fig. 5 RC joint model proposed by Youssef and Ghobarah (2001)

joint was determined using the softened truss model theory. Youssef and Ghobarah (2001) then proposed a more refined model that can simulate joint shear behavior as well as bond slip near the joint region (Fig. 5). The shear behavior of a joint was represented by four rigid elements enclosing the joint core (pin-connected to one another) and two nonlinear axial springs connecting the diagonals of the joint. The axial spring deformations corresponding to a specific joint shear deformation were determined considering the deformed shape, and the axial spring forces were computed using static equilibrium conditions. However, these two studies (Biddah and Ghobarah 1999, Youssef and Ghobarah 2001) did not well address typical RC hysteretic behavioral characteristics such as strength degradation, stiffness degradation, and/or pinching.

Other approaches taken to this problem have included applying the finite element method (Pantazopoulou and Bonacci 1994, Fleury *et al.* 1999), and using a continuum-type model having a twelve-node joint element and four ten-node transient elements, one for each boundary of the joint (Elmorsi *et al.* 1998). Finally, Lowes and Altoontash (2002) proposed a joint shear panel model having four interface-shear springs and eight bar-slip springs (one interface-shear spring and two bar-slip springs at each rigid boundary of the joint), specifically for older non-ductile frames without joint reinforcement.

3. RC beam-column joint behavior

The shear stress vs. shear deformation relationship of RC beam-column joints subjected to cyclic lateral loading is characterized based on connection tests conducted by the authors, as well as other tests reported in the literature. The joint shear failure mechanism is described in terms of physical phenomena such as concrete damage and reinforcement yielding. An analytical method for estimating nonlinear hysteretic joint shear behavior is then presented.

3.1 Experimental results for joint shear behavior

The authors tested four cruciform RC beam-column-slab subassemblies (two concentric and two eccentric connections) subjected to quasi-static cyclic lateral loading. Each subassembly represented a 2/3-scale edge connection in an exterior moment-resisting frame, isolated at assumed inflection points between floors and between column lines. Fig. 6 shows typical elevation and plan views for the specimens, and Fig. 7 illustrates important reinforcement details. Each specimen consisted of a column, two edge-beams framing into opposite faces of the column, and a transverse beam and floor slab on one side only. The column pin-to-pin story height (l_c) was 3.0 m, while the beam pin-to-pin span length (l_b) was 5.0 m. The specimens were generally proportioned based on current design code requirements (ACI 318-02 2002) and recommendations (ACI 352R-02 2002). During testing (up to a maximum of 6% story drift), all four specimens underwent some beam plastic hinging, while three of the specimens (all except SL3) eventually exhibited joint shear failure. Details of the experimental program and test results can be found elsewhere (Shin and LaFave 2004a, 2004b).

The typical relationship between average joint shear stress (τ_j) and average joint shear deformation, or strain, (γ) in RCMRF structures was investigated based on numerous laboratory connection tests. For example, Fig. 8 shows the hysteretic $\tau_j - \gamma$ curves of specimens SL2 and SL4, obtained from the authors' tests; other tests generally showed similar patterns of cyclic joint shear

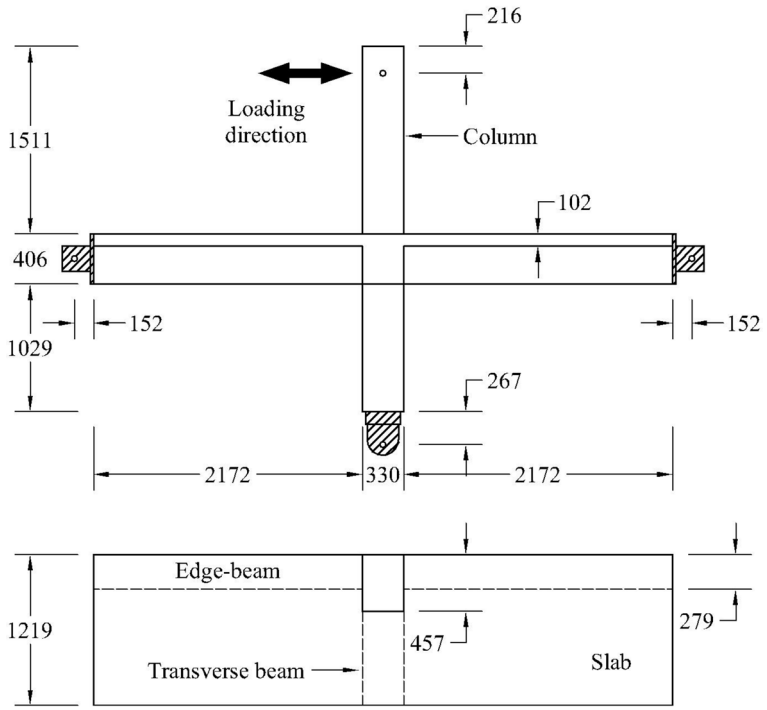

Fig. 6 Elevation and plan views of specimen SL1 (units: mm)

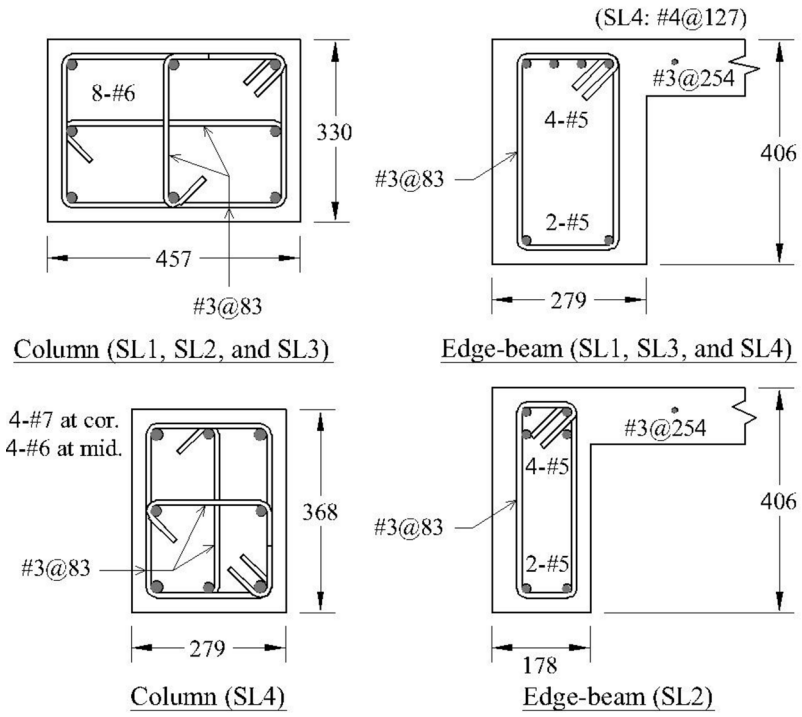

Fig. 7 Reinforcement details (units: mm)

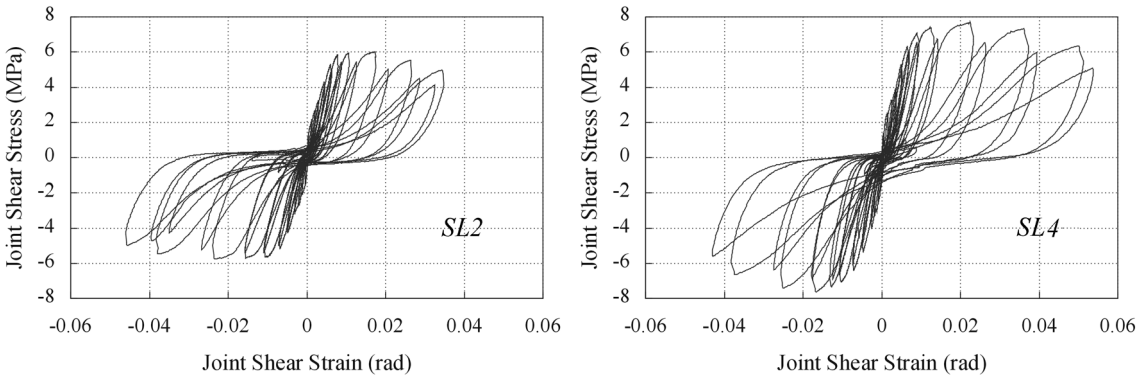

Fig. 8 Hysteretic joint shear stress vs. strain curves

behavior. Average joint shear stress was determined by dividing the horizontal joint shear force by the product of column depth and effective joint width (equal to the average of the beam and column widths). Joint shear forces were calculated considering column shear forces and beam moments applied at the joint boundaries. Average joint shear deformation was determined using data measured by LVDTs installed extending over the entire exterior joint face.

3.1.1 Monotonic (envelope) response

Fig. 9(a) plots envelope $\tau_j - \gamma$ curves for specimens SL1 through SL4, constructed by connecting the peak drift point of each cycle. In specimens that ultimately fail by joint shear (such as SL1, SL2, and SL4), the envelope $\tau_j - \gamma$ curves are fairly smooth, but they can be simplified (for use in analysis) as four linear segments, starting from the origin and connecting three key points, so-called as *joint shear cracking* (γ_{cr}, τ_{jcr}), *reinforcement yielding* (γ_y, τ_{jy}), and *joint shear strength* (γ_m, τ_{jm}), as described in Fig. 9(b). (After the point of joint shear strength, the envelope curves typically show gradually descending inclination; this part of the envelope curve can be represented by a straight

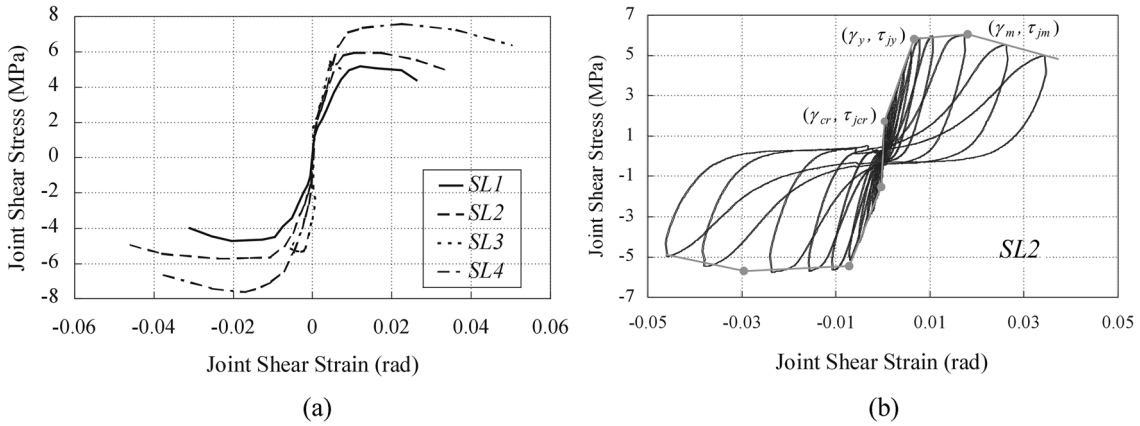

Fig. 9 (a) Envelope joint shear stress vs. strain curves, (b) Simplified envelope joint shear stress vs. strain relationship

line with a modest negative slope.) In the case of joint shear failure *after* beam hinging (as in SL1, SL2, and SL4), the second key point has been found to correspond to longitudinal beam bar yielding (Shin and LaFave 2004b). In the case of joint shear failure *without* prior beam hinging, the joint reinforcement typically yields near the second key point. (Joint shear failure is defined as a condition wherein a joint cannot resist higher joint shear stress; this condition occurs at the third key point, joint shear strength.)

Table 1 Key point ordinates for experimental joint shear stress vs. strain curves

Specimen		f_c' (MPa)	$\frac{\rho_j f_{yj}}{\sqrt{f_c'}}$ (√MPa)	$\frac{N_c}{A_c f_c'}$	Failure mode	Experimental results				
						τ_{jy} (MPa)	τ_{jm} (MPa)	γ_y (rad)	γ_m (rad)	Post-peak slope (MPa/rad)
Fujii & Morita (1991)	A4	40.1	0.68	0.23	J	9.4	10.1	0.007	0.028	–52
Kurose *et al.*[1] (1991)	J1	24.1	0.84	0.00	BJ	7.8	8.7	0.009	0.035	N.A.
Leon (1990)	BCJ2	27.6	0.35	0.00	BJ	5.3	6.1	0.004	N.A.	N.A.
	BCJ3	27.6	0.35	0.00	BJ	5.5	6.8	0.003	N.A.	N.A.
Meinheit & Jirsa (1981)	12	35.2	1.70	0.30	BJ	13.7	14.0	0.007	0.012	–191
	13	41.3	0.98	0.25	J	10.8	11.2	0.005	0.010	–181
	14	33.2	0.79	0.32	J	10.3	10.8	0.010	0.020	–85
Noguchi & Kashiwazaki (1992)	OKJ-1	70.0	0.86	0.12	BJ	12.5	14.2	0.005	0.010	–137
	OKJ-4	70.0	0.86	0.12	BJ	12.5	15.0	0.004	0.021	0
	OKJ-5	70.0	0.86	0.12	J	13.0	14.8	0.006	0.018	–394
	OKJ-6	53.5	0.98	0.12	J	11.5	13.1	0.006	0.015	N.A.
Raffaelle & Wight (1995)	1 (RW1)	28.6	0.68	0.02	BJ	5.2	6.0	0.004	0.014	–25
	2	26.8	0.70	0.03	BJ	4.1	4.4	0.006	0.014	–57
	3	37.7	0.59	0.02	BJ	4.0	4.9	0.005	0.017	–38
	4	19.3	0.83	0.04	BJ	3.5	4.2	0.005	0.018	–51
Shin & LaFave[2] (2004b)	SL1	29.9	0.48	0.00	BJ	4.9	5.3	0.009	0.016	–53
	SL2	36.2	0.44	0.00	BJ	5.8	6.2	0.007	0.021	–53
	SL4	31.2	0.96	0.00	BJ	7.1	7.7	0.008	0.020	–46
Teng & Zhou (2003)	S1	33.0	0.60	0.11	BJ	8.0	8.6	0.005	0.010	–98
	S2	34.0	0.59	0.11	BJ	8.0	8.6	0.007	0.013	–119
	S3	35.0	0.58	0.10	BJ	8.0	8.3	0.010	0.022	–139
	S5	39.0	0.83	0.11	BJ	6.5	7.5	0.007	0.007	N.A.
	S6	38.0	0.84	0.11	BJ	6.5	7.3	0.007	0.015	–99
Watanabe *et al.* (1988)	WJ-1	29.2	0.89	0.07	BJ	8.8	8.8	0.003	0.007	–138
	WJ-3	29.2	0.89	0.07	BJ	8.8	10.2	0.002	0.008	–157
	WJ-6	29.2	0.89	0.07	J	11.7	12.5	0.004	0.007	–143

Note: Each of the indicated specimens has (1) floor slabs on both sides and (2) a floor slab and transverse beam on one side only. N.A. means “not available”.

Table 1 summarizes several connection parameters and key point ordinates for the envelope $\tau_j - \gamma$ curves determined from the authors' connection tests and from other tests reported in the literature (which showed joint shear failure and which provided joint shear deformation data in addition to joint shear stress data). The authors found more than fifty tests falling into this category, but only specimens with at least half of the required cross-sectional area of joint transverse reinforcement (A_{sh}) per ACI 318-02 (at a spacing no greater than the limiting value) were considered in this study. All twenty-six specimens in the table were isolated cruciform (interior) connections, and a few of them included either a transverse beam and/or floor slab, as noted below the table. The specimens were tested under uni-directional quasi-static cyclic lateral loading, typically up to a maximum of 4% to 6% story drift; all of the tabulated specimens eventually failed due to joint shear, although some of them first underwent beam hinging.

Table 1 lists the volumetric ratio of joint reinforcement (ρ_j) times the joint reinforcement yield strength (f_{yj}), normalized by the square root of the concrete compressive strength (f_c'); this is a comparative measure of the relative amount of joint reinforcement among the specimens. (Note that dimensionally correct units are consistently used for computing and reporting such values throughout this paper; ACI 318-02 and ACI 352R-02, on the other hand, define the term $\sqrt{f'_c}$ to have units of "MPa".) Here, ρ_j is defined as the total cross-sectional area of joint transverse (hoop and crosstie) reinforcement in a layer (A_{sh}) divided by the vertical spacing (s) times the column width (b_c).

Table 1 also lists the column axial load (N_c) divided by the column gross cross-sectional area (A_c), normalized by the concrete compressive strength (f_c'). With respect to reinforcement bond conditions in the joints, the column depth to beam bar diameter ratio ranged from about 11 to 30 in the specimens, with an average of 21 and a standard deviation of 4.5. As for the failure mode notation, "J" stands for joint shear failure *without* beam hinging, while "BJ" indicates joint shear failure *after* beam hinging. The reported joint shear stress values were determined by dividing the horizontal joint shear force by the product of column depth and effective joint width (equal to the average of the beam and column widths). The joint shear stresses were the larger of the positive and negative values, while the joint shear strains and post-peak slopes were an average of the positive and negative values. The key point ordinates are greatly scattered due to the different failure modes, various joint details, and the range of material properties used; there do not seem to be any clear trends in these key point ordinates with respect to the tabulated connection parameters.

The joint shear stress at shear crack initiation, τ_{jcr}, varied widely with concrete strength and column axial load, and the γ_{cr} value was typically very small (on the order of 0.0005 radians); τ_{jcr} and γ_{cr} values are not included in the table due to lack of consistent data. The γ_y values ranged from 0.002 to 0.010 radians, and γ_m was typically between 0.01 and 0.03 radians. (For most of the specimens, 0.01 radians of joint shear deformation alone would produce nearly 1% story drift.) The τ_{jy} values were approximately equal to 90% of τ_{jm} (the joint shear stress when the joint shear strength had been reached). The average of the τ_{jm} values, when normalized by the square root of the concrete compressive strength, was about $1.85\sqrt{}$MPa in J-type failure mode specimens, while it was about 20% less in BJ-type failure mode specimens. After the point of joint shear strength (γ_m, τ_{jm}), the envelope $\tau_j - \gamma$ curves typically became flat or showed slightly descending inclination; the slope of this part (called the "post-peak slope" in Table 1) ranged from zero (horizontal) on up to about half of the average (secant) ascending slope from the origin to the point of joint shear strength; the average descending slope was about 15% of the secant ascending slope. The largest joint shear deformations reached during the tests (including behavior after the joint shear strength

had been reached) were typically about 0.03 to 0.05 radians.

Some researchers (Fujii and Morita 1991, Teraoka and Fujii 2000) have proposed fixed values (0.005 and 0.028 radians; 0.004 and 0.01 radians, respectively) for the joint shear strains corresponding to the "reinforcement yielding" and "joint shear strength" points. However, using fixed values for the key strain points, regardless of joint details, is not reasonable in light of the above observations; therefore, a rational approach to estimate the envelope $\tau_j - \gamma$ curve of any given joint is preferred.

3.1.2 Hysteretic properties

As can be seen in Fig. 8, cyclic $\tau_j - \gamma$ curves commonly exhibit pinching (the middle part of each hysteretic loop is relatively narrow), as well as stiffness and strength degradation (typically noted by comparing consecutive same-drift cycles). These are characteristic phenomena that also occur in plastic hinge regions of RC frame members. In joints, this behavior has mostly been attributed to shear transfer across inclined joint concrete cracks. In general, these hysteretic characteristics are negligible before joints experience initial shear cracking. Degradation of stiffness and strength greatly increases after the point of reinforcement yielding, and the extent of pinching spreads as joints are subjected to larger shear deformation cycles. The degree of each hysteretic characteristic was somewhat scattered from one specimen to another, regardless of specimen damage stages.

3.2 Description of joint shear failure mechanisms

From the RC beam-column connection tests described above, it has been found that, before initial joint shear cracking occurs, a joint behaves elastically and the $\tau_j - \gamma$ curve is almost linear. At the point of joint shear cracking, a joint starts to exhibit inclined shear cracks (which initially may not even be visible); the cracks diagonally intersect one another due to reversed loading. As a result of the cracking process, the envelope $\tau_j - \gamma$ curve experiences gradual stiffness loss. The point of reinforcement yielding corresponds to yielding of horizontal joint reinforcement (in the case of joint shear failure *without* beam hinging) or yielding of longitudinal beam bars (in the case of joint shear failure *after* beam hinging). From this point, the envelope $\tau_j - \gamma$ curve begins to show rapid stiffness loss. In the case of joint shear failure after beam hinging, joint reinforcement yields between the points labeled as "reinforcement yielding" and "joint shear strength" (more description of this case is presented later). Few new joint shear cracks occur after joint reinforcement yielding, but crack widths quickly become larger and joint cracks no longer close completely at the zero load point, due in part to residual strains in the joint reinforcement.

At the point of joint shear strength, a joint reaches its maximum load-carrying capacity. At about this point, joint shell concrete starts to spall off due to extensive crossing of the inclined cracks, and the joint undergoes concrete compression failure. The envelope $\tau_j - \gamma$ curve shows a negative inclination from this point onward, meaning that the joint shear strength gradually decays. Joint concrete crushing (joint shear failure) typically occurs after joint reinforcement yielding, as concluded by Bonacci and Pantazopoulou (1993), who investigated the effect of the amount of joint reinforcement on joint shear resistance in beam-column connections. Also, Stevens *et al.* (1991) suggested that if RC is subjected to repeat cycles of shear stress at any level above that which causes reinforcement yielding, the principal tensile strain will continue to increase with each repeat cycle, causing the concrete compressive strength to decrease until failure eventually occurs by concrete crushing.

In the case of joint shear failure after beam hinging, rapid stiffness loss in the envelope $\tau_j - \gamma$ curve results indirectly from beam hinging occurring near the joint, in part because the joint core starts to dilate faster after losing some confinement (that had been provided by the beams), due to large flexural cracks at beam/joint interfaces. Although the joint shear strength may be somewhat higher than the joint shear demand at the time beam hinging occurs, this strength decays under subsequent cyclic loading (of similar joint shear inputs) and can eventually become smaller than the joint shear demand imposed at beam hinging, resulting in joint shear failure (Joh *et al.* 1991, Kitayama *et al.* 1991, Kitayama 1992). Furthermore, the concrete strut may be required to resist a larger portion of the total joint shear (in other words, the net demand on the concrete strut may increase) when the bond condition along longitudinal beam bars deteriorates, especially after beam hinging (Kitayama *et al.* 1991).

In some previous RC connection tests, beam hinging did not lead to large joint shear deformations (or to joint shear failure), even when the joints were subjected to numerous subsequent displacement reversals (Bonacci and Pantazopoulou 1993), as in specimen SL3 tested by the authors. The joint shear stress demands seen in those specimens (which had beam hinging without further progressive joint damage) were generally lower than the ones reached in specimens that showed either J-type or BJ-type failure modes.

Although RC joint shear response is somewhat influenced by the connection failure mode, the joint shear stress and/or strain levels occurring in specimens that failed in a J-type mode were usually similar to (or slightly higher than) those in companion specimens that failed in a BJ-type mode. This phenomenon has been observed in many connection tests conducted on specimens designed following modern code requirements. Therefore, possible small differences in joint shear behavior between beam-column connections that failed in the two different modes have been neglected for modeling purposes in this study.

3.3 Analytical solution for joint shear behavior

As a general solution scheme, the key point ordinates of an RC beam-column connection envelope $\tau_j - \gamma$ curve can be approximately obtained by employing the modified compression field theory (MCFT) developed by Vecchio and Collins (1986). An RC joint core is considered as a two-dimensional (2-D) concrete panel element with uniformly distributed orthogonal reinforcement; the joint transverse reinforcement and the longitudinal column bars are regarded as the distributed horizontal and vertical reinforcement, respectively. Presuming that the middle region of a joint (away from the longitudinal beam bars) limits joint shear strength and controls the joint shear failure mechanism, the volumetric steel ratio of horizontal reinforcement (ρ_x) was taken as the total cross-sectional area of joint transverse reinforcement in a layer divided by the product of vertical spacing and column width. The volumetric steel ratio of vertical reinforcement (ρ_y), which was taken as the total cross-sectional area of longitudinal column bars divided by the product of column width and column depth, was typically two to five times larger than that of horizontal reinforcement, so the analytical joint shear behavior was governed by the horizontal reinforcement in most cases.

Fig. 10 explains the equilibrium equations, compatibility conditions, and material constitutive laws used for these analyses (note that "v_{xy}" is the average shear stress, equivalent to τ_j). In keeping with the MCFT, it is assumed that: (1) principal stress directions in the concrete coincide with principal strain directions, (2) average concrete strain in the direction of reinforcement is equal to average

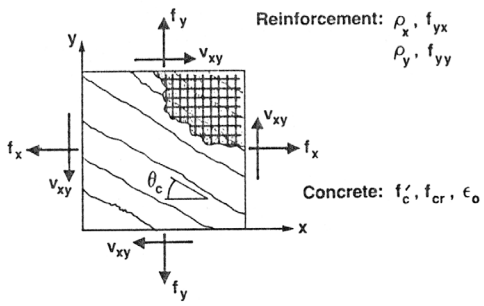

(a) Cracked reinforced concrete element

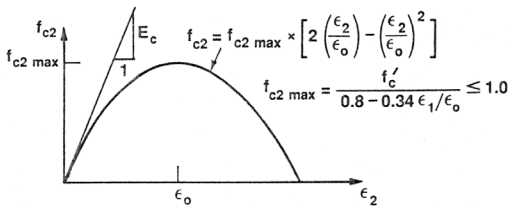

(d) Concrete in principal compressive direction

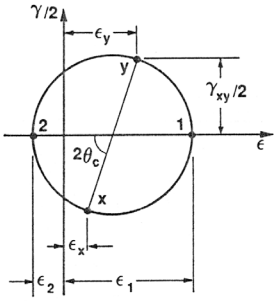

(b) Mohr's circle of average strains

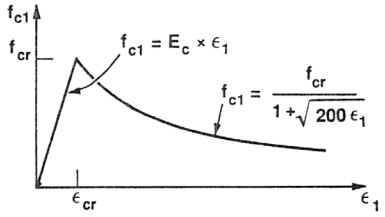

(e) Concrete in principal tensile direction

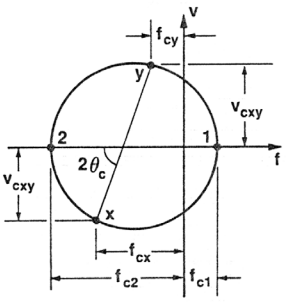

(c) Mohr's circle of average concrete stresses

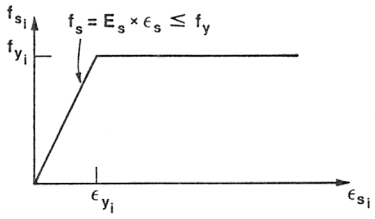

(f) Reinforcing steel

Fig. 10 Modified compression field theory proposed by Vecchio and Collins (1986)

reinforcement strain, and (3) reinforcing steel does not resist shear (dowel action is neglected). Additionally, to simplify the analysis process, a joint core is assumed to be under uniform in-plane stress along each of the joint boundaries, as proposed by Vecchio and Collins (1988) who applied the MCFT for predicting the response of RC beams; actual stress conditions in a joint will vary locally at each particular loading stage (because every joint boundary is actually under coupled compressive and tensile forces transmitted from the top and bottom (or left and right) of each beam (or column)). Then, the monotonic joint shear stress (τ_j) vs. strain (γ) relationship may be acquired for a given set of average normal (axial) stresses at the joint boundaries.

According to Collins and Mitchell (1991), concrete cracking starts when the principal tensile stress in the joint concrete (f_{c1}) reaches its proportional limit with respect to the principal tensile strain (ε_1):

$$f_{c1} = \begin{cases} E_c \cdot \varepsilon_1 & (\varepsilon_1 \le \varepsilon_{cr}) \\ \dfrac{\alpha_1 \cdot \alpha_2 \cdot f_{cr}}{1 + \sqrt{500\varepsilon_1}} & (\varepsilon_1 > \varepsilon_{cr}) \end{cases} \tag{1}$$

Here, E_c is the modulus of elasticity of concrete (initial tangent stiffness equal to $2f_c'/\varepsilon_o$); ε_o is the strain in concrete corresponding to the concrete compressive strength (f_c') from a standard cylinder test; f_{cr} is the concrete (tensile) cracking stress, taken as 0.5 times the square root of f_c' (in MPa); ε_{cr} is the concrete cracking strain computed by f_{cr}/E_c; and α_1 and α_2 are factors accounting for bond characteristics of the reinforcement and type of loading, respectively. As joint boundary stresses get higher, the compressive strength of joint concrete ($f_{c2\max}$) decays with increasing principal tensile strain (ε_1) in the transverse direction:

$$f_{c2\max} = \frac{f_c'}{0.8 - 0.34\varepsilon_1/\varepsilon_o} \le f_c' \tag{2}$$

The analysis stops when the principal compressive stress in concrete (f_{c2}) exceeds the reduced concrete compressive strength ($f_{c2\max}$); in other words, the analysis cannot compute further joint shear response after the joint concrete reaches compression failure. Further details of the analysis procedures employed for acquiring the monotonic $\tau_j - \gamma$ curve of an RC joint under a given set of normal stresses can be found in the Appendix of Vecchio and Collins (1986).

Fig. 11 compares analytically computed envelope $\tau_j - \gamma$ curves with experimentally determined ones for six RC beam-column connections from Table 1. SL1 and SL4 had a transverse beam and floor slab on one side only, while the other specimens were bare cruciform connections. A4 and OKJ-5 failed in a J-type mode, while the other specimens failed in a BJ-type mode. (No specimen with a floor slab that failed in a J-type mode and that reported joint shear deformation data was found in the literature.) Solid and dashed lines in each figure indicate (positive) experimental and analytical results, respectively, and key point ordinates for the analytical results are marked with dots. As mentioned earlier, the MCFT cannot compute further joint shear response after the joint concrete reaches compression failure. Thus, this part of the analytical joint shear stress vs. strain curve is assumed to be a straight line with a negative slope equal to 5% of the secant ascending slope up to the joint shear strength point; the descending slope is set to a somewhat smaller value than the average from the test results listed in Table 1, considering that the analytical joint shear strain at the joint shear strength point is typically a bit less than the experimental one, as explained later. This line forms the fourth segment of the quad-linear analytical envelope curve, as plotted in Fig. 11. In all six cases, the analysis results generally match the experimental ones quite well.

Analytically determined key point ordinates for all of the specimens from Table 1, including values for the above six specimens, are summarized in Table 2. The analytical τ_{jy} and τ_{jm} values were, on average, approximately 95% of the experimental ones, while the analytical γ_y and γ_m values were on average somewhat different from (about 125% and 75% of) the experimental ones.

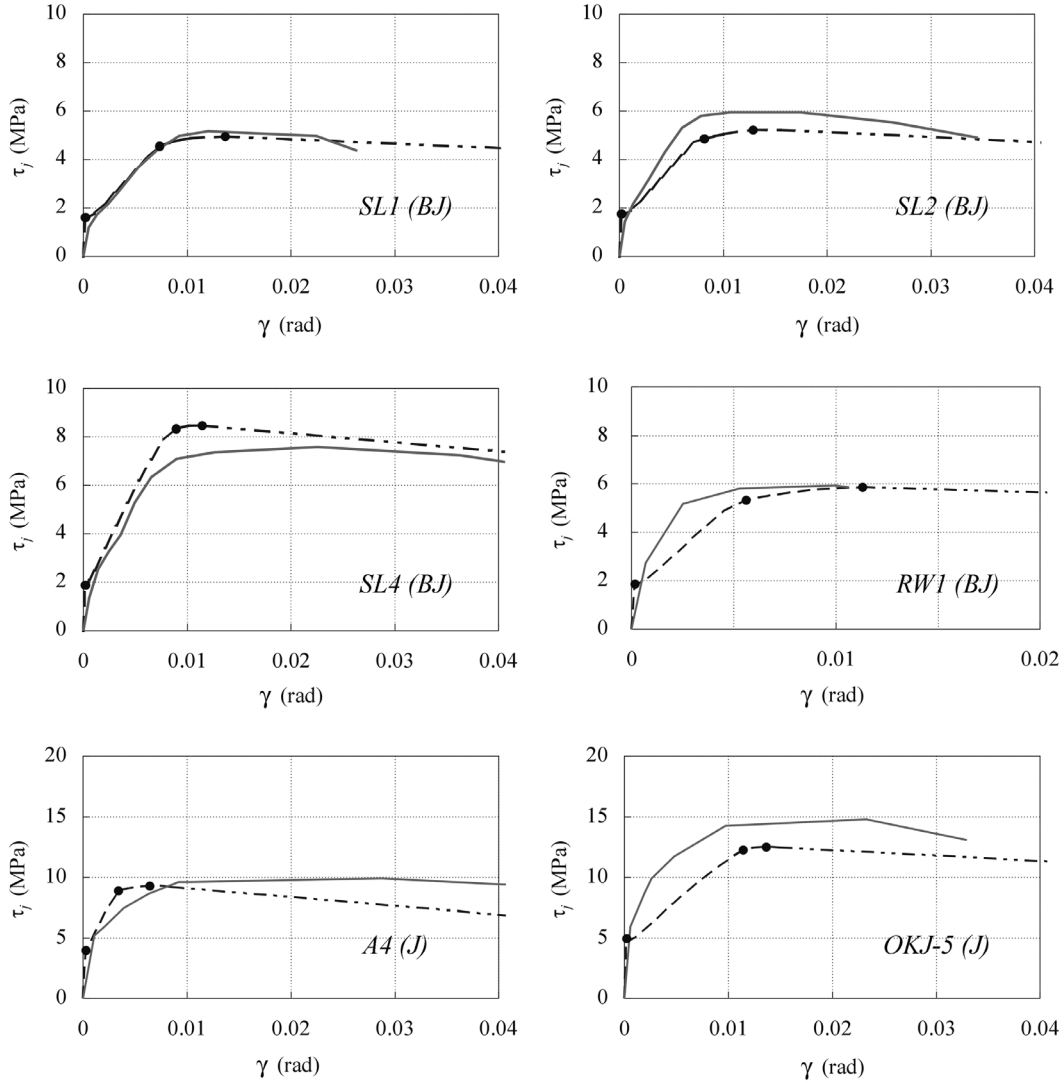

Fig. 11 Comparison between analytical and experimental envelope $\tau_j - \gamma$ curves (dashed and solid lines represent analytical and experimental results, respectively)

It was concluded that the proposed analytical scheme generally gave good (and slightly conservative) solutions for computing the joint shear stress vs. strain responses of RC beam-column connections.

In combination with the analytically computed and simplified (quad–linear) envelope $\tau_j - \gamma$ curve, an appropriate hysteretic model (proposed by Foutch *et al.* 2003) is adopted and calibrated to reproduce hysteretic characteristics of the experimental joint shear behavior, as presented in a later section.

Table 2 Key point ordinates for analytical joint shear stress vs. strain curves

Specimen		Analytical results					
		τ_{jcr} (MPa)	τ_{jy} (MPa)	τ_{jm} (MPa)	γ_{cr} (rad)	γ_y (rad)	γ_m (rad)
Fujii & Morita (1991)	A4	4.0	8.9	9.3	0.0003	0.003	0.006
Kurose *et al.* (1991)	J1	2.3	5.9	6.0	0.0002	0.007	0.009
Leon (1990)	BCJ2	1.6	4.1	4.6	0.0002	0.004	0.011
	BCJ3	1.5	4.0	4.5	0.0002	0.004	0.011
Meinheit & Jirsa (1981)	12	4.5	N.A.	13.7	0.0003	N.A.	0.005
	13	4.6	N.A.	14.9	0.0003	N.A.	0.006
	14	4.3	N.A.	12.0	0.0003	N.A.	0.006
Noguchi & Kashiwazaki (1992)	OKJ-1	5.0	11.9	12.2	0.0002	0.011	0.015
	OKJ-4	5.0	11.9	12.2	0.0002	0.011	0.015
	OKJ-5	5.0	12.3	12.5	0.0002	0.011	0.014
	OKJ-6	4.1	N.A.	10.7	0.0002	N.A.	0.012
Raffaelle & Wight (1995)	1 (RW1)	1.9	5.3	5.9	0.0002	0.006	0.011
	2	1.8	5.3	5.7	0.0002	0.006	0.010
	3	2.1	5.5	6.3	0.0002	0.005	0.012
	4	1.6	5.0	5.1	0.0002	0.006	0.008
Shin & LaFave (2004b)	SL1	1.6	4.6	5.0	0.0002	0.007	0.014
	SL2	1.8	4.9	5.2	0.0002	0.008	0.013
	SL4	1.9	8.3	8.5	0.0002	0.009	0.011
Teng & Zhou (2003)	S1	2.8	6.3	6.8	0.0002	0.004	0.008
	S2	2.8	6.4	6.8	0.0002	0.004	0.009
	S3	2.9	6.4	6.9	0.0002	0.004	0.009
	S5	2.8	8.4	9.0	0.0002	0.005	0.009
	S6	2.7	8.4	8.9	0.0002	0.005	0.008
Watanabe *et al.* (1988)	WJ-1	2.3	6.8	7.3	0.0002	0.005	0.008
	WJ-3	2.3	6.7	7.3	0.0002	0.005	0.008
	WJ-6	2.3	7.2	7.6	0.0002	0.005	0.007

4. Modeling of beam-column connection subassemblies

Modeling of RC beam-column connection subassemblies subjected to cyclic lateral loading is presented in this section, explicitly incorporating hysteretic joint shear behavior, as well as other appropriate inelastic behavior occurring in and around the connection. The hysteretic joint shear behavior consists of a monotonic (envelope) joint shear response analytically computed by the MCFT, and hysteretic properties calibrated based on experimental data. It is further assumed that all inelastic beam and column deformations occur in the vicinity of beam/joint or column/joint interfaces.

4.1 Element configuration in proposed connection model

Fig. 12 illustrates a DRAIN-2DX (nonlinear structural analysis program; Prakash *et al.* 1993) computer model for a typical cruciform RC beam-column connection subassembly subjected to lateral loading. The joint is represented by four rigid link elements located along the joint edges and three nonlinear rotational springs embedded in one of the four hinges connecting adjacent rigid elements. DRAIN-2DX Element 10 developed by Foutch *et al.* (2003), which is a modified version of DRAIN-2DX Element 04 (simple connection element linking two nodes with an identical coordinate set), is used for the nonlinear rotational springs at the joint. (Element 10 has several different hysteretic models that could be applied to either steel or RC structures; to date, the element has primarily been used by the developers for analyzing steel structures.) A single Element 10 can express a bi-linear moment vs. rotation relationship as a primary curve, and it can incorporate typical hysteretic properties such as stiffness degradation, strength degradation, and pinching (Fig. 13). In this study, three such springs connected in parallel are used to represent hysteretic joint shear behavior. The hysteretic joint shear force (V_j) vs. strain (γ) curve is first determined from a hysteretic $\tau_j - \gamma$ curve described by the analytically computed and simplified (quad-linear) envelope; V_j is calculated by multiplying the joint shear stress (τ_j) by the product of column depth and effective joint width (average of the beam and column widths). Then the hysteretic moment (M_s) vs. rotation (θ_s) curve to be expressed by the combination of the three joint springs is acquired from the joint shear force (V_j) vs. strain (γ) curve by:

$$\theta_s = \gamma\,;\; M_s = V_j \cdot jd \tag{3}$$

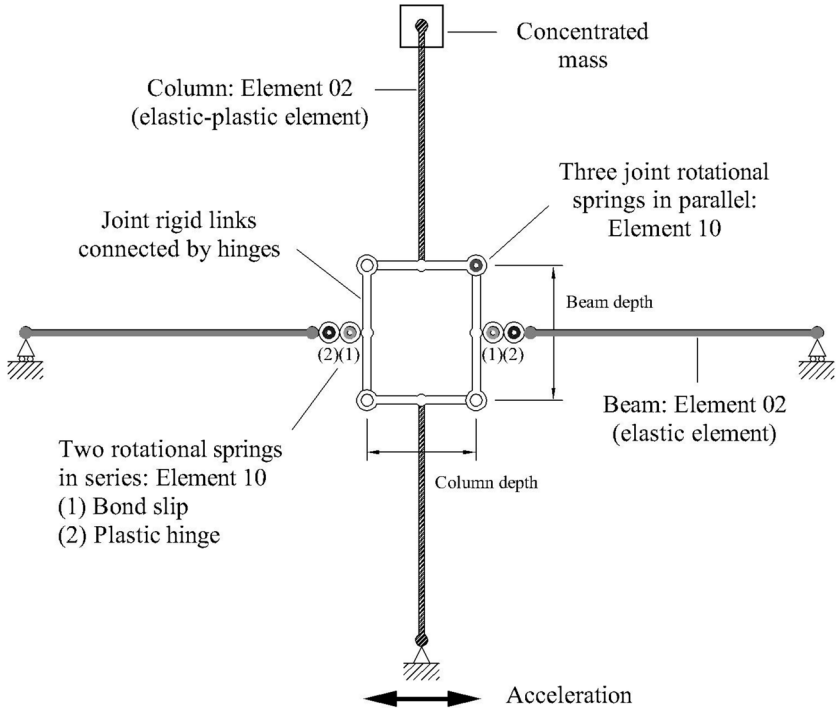

Fig. 12 DRAIN-2DX model for a beam-column connection subassembly

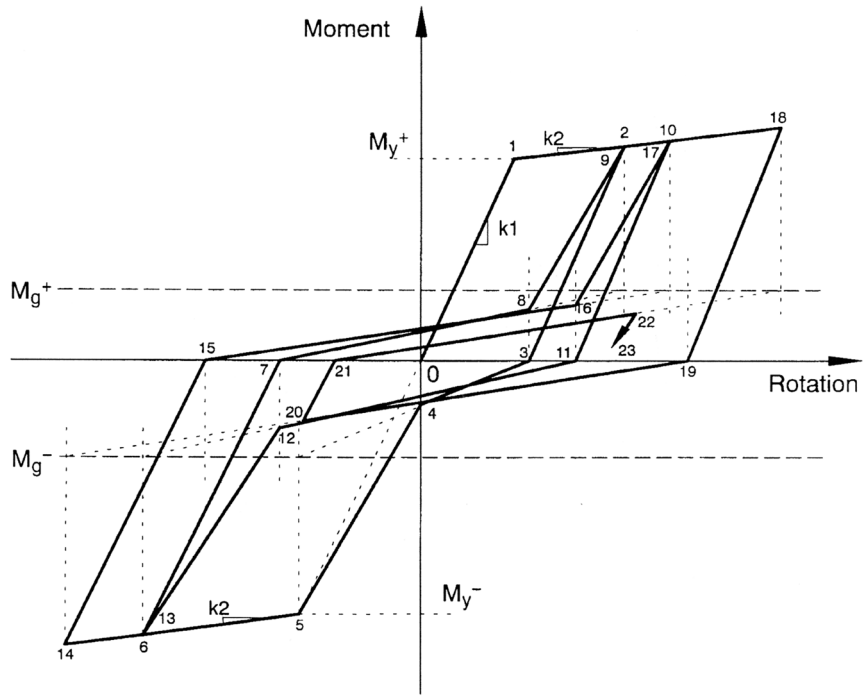

Fig. 13 Hysteretic behavior of DRAIN-2DX Element 10 per Foutch *et al.* (2003)

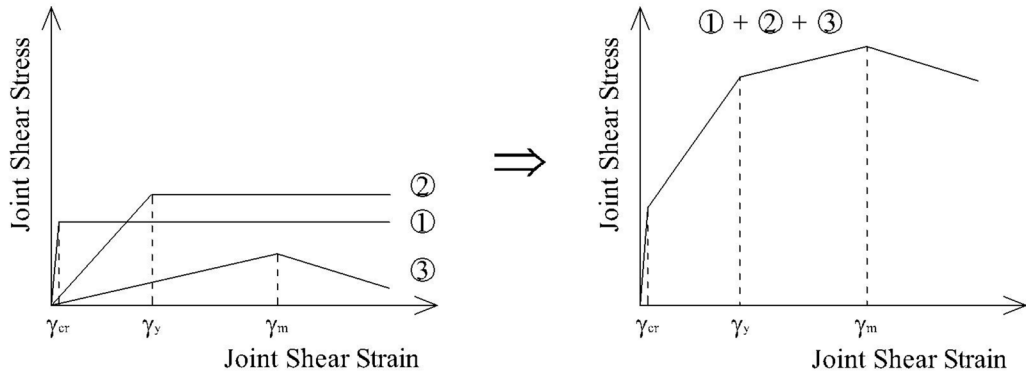

Fig. 14 Combination of three bilinear joint springs in parallel

Here, *jd* is assumed to be the average of positive and negative beam moment arms at beam/joint interfaces. Fig. 14 illustrates the way the three joint springs (each with a bilinear envelope) combine to express a quad-linear envelope $M_s - \theta_s$ curve. Two of the springs are elastic and then perfectly plastic, while the third spring has a negative second slope equal to that of the fourth linear segment in the quad-linear envelope $M_s - \theta_s$ curve.

Outside of the joint itself, each (upper and lower) column is modeled using one DRAIN-2DX Element 02, which consists of an elastic-perfectly plastic component and a strain-hardening (elastic)

component in parallel (and Element 02 can account for axial force (P) and moment (M) interaction). Each beam is modeled using Element 02 for the elastic part and two of Element 10 for the nonlinear rotational springs located at the beam/joint interface; the three elements are connected in series. One of the nonlinear rotational springs represents fixed end rotations arising at the beam/joint interface due to bond slip and yielding of longitudinal beam bars in the joint, while the other represents plastic hinge rotations near the end of the beam. The vertical position of the beam elements and the horizontal position of the column elements are simply located at the beam mid-depth and the column mid-depth, respectively. This beam model is similar to one proposed by Filippou *et al.* (1999), which consisted of three sub-elements (elastic, spread plastic, and interface bond-slip) connected in series. However, Filippou *et al.* did not address hysteretic joint shear behavior, assuming that joints could be designed and detailed in order that joint shear deformations would remain small.

4.2 Details for joint modeling

The necessary input parameters for Element 10 are initial stiffness ($k1$), strain-hardening ratio ($k2/k1$), positive and negative yield moments (M_y^+ and M_y^-), strength degradation factor, and positive and negative pinching moments (M_g^+ and M_g^-), as illustrated in Fig. 13. The strength degradation factor is defined as the ratio of the second to the first cycle moment at the maximum rotation reached during the first cycle, for two consecutive loading cycles (for example, the ratio between moments at the points labeled as "9" and "2" in Fig. 13). The positive and negative pinching moments determine the extent of pinching in the middle part of each hysteretic loop, by designating the direction of reloading branches in conjunction with the maximum rotations reached during the previous cycle (for example, the negative pinching moment in Fig. 13 specifies the slope of the line connecting the points labeled as "3" and "4"). The extent of stiffness degradation during reloading is necessarily determined from assigning pinching moments, while stiffness during unloading is kept as a constant value equal to the initial stiffness ($k1$).

All input parameters for the three joint rotational springs, except the strength degradation factors and the M_g^+ and M_g^- values, are determined from the quad-linear envelope $M_s - \theta_s$ curve, with $k2/k1$ values for the first two springs set to zero (see Fig. 14). For the two elastic and perfectly plastic springs, the strength degradation factor is specified as 0.95 and the pinching moments are assumed as one-fifth of the yielding moments of each spring, while neither strength degradation nor pinching is considered for the third spring (with a negative $k2/k1$ value); values for these two parameters have been approximately determined from investigating the test results of the specimens listed in Table 1. The positive and negative input values for each joint spring are identical because the $\tau_j - \gamma$ curves are assumed symmetric for positive and negative loading.

Fig. 15 compares the analytical and experimental joint shear response of specimen SL4; the analysis was conducted using a quasi-static displacement history simulating the peak experimental joint shear deformation of each cycle. The analytical result agrees well with the experimental one in terms of the extent of pinching and the energy dissipated in each cycle, as well as from the standpoint of envelope properties; however, the joint model could not smoothly replicate overall stiffness degradation. In general, the analytical joint model was also able to well represent the experimental joint shear behavior of the other beam-column connection subassemblies listed in Tables 1 and 2.

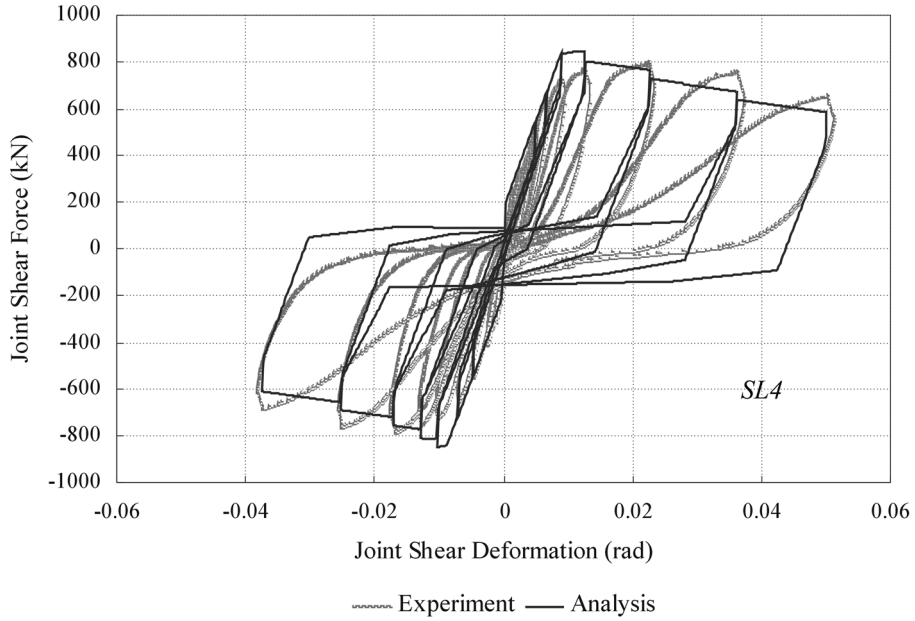

Fig. 15 Comparison of hysteretic joint shear responses from test and analysis

4.3 Details for beam and column modeling

The stiffness input parameters for Element 02 are the concrete elastic modulus, section moment-of-inertia, cross-sectional area, and strain-hardening ratio (ratio of post-yield slope to pre-yield slope of the moment-curvature diagram). The modulus of elasticity for concrete (E_c) was estimated from the cylinder test results by the ACI 318-02 equation:

$$E_c(\text{MPa}) = 4730\sqrt{f_c'(\text{MPa})} \tag{4}$$

In keeping with Paulay and Priestley (1992) recommendations, the column moment-of-inertia (I_c) is taken as half the gross moment-of-inertia for columns with low axial load (when average column axial stress normalized by concrete compressive strength is less than 0.2); otherwise 70% of the gross moment-of-inertia is used. The beam moment-of-inertia (I_b) is taken as 35% of the gross moment-of-inertia, computed considering the effective slab width per ACI 318-02. Gross column and beam cross-sectional areas are used. The strain-hardening ratio for the columns is computed based on yield and nominal moments and curvatures from the column moment-curvature diagram; the strain-hardening ratio for the beam elastic elements is not utilized.

The column strength input parameters for Element 02 are positive and negative yield moments, compression and tension yield forces, and positive and negative balanced points of the P-M interaction curve. The beam (elastic part) strength input parameters for Element 02 are only positive and negative yield moments, which are set to very large values in order to lump all inelastic deformations at the bond slip and plastic hinge rotational springs.

For the input parameters of the moment vs. rotation relationship of the beam plastic hinge spring, the initial stiffness is assigned a large value in order to generate no rotation before yielding, and the

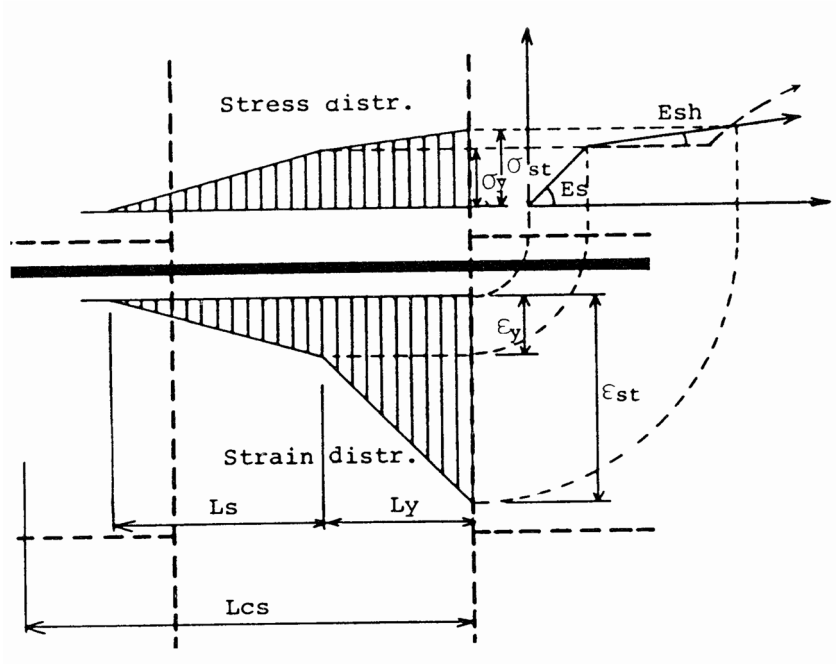

Fig. 16 Stress and strain distributions (after yielding) assumed by Morita and Kaku (1984)

strain-hardening ratio is set to a value equivalent to 0.03 times $6E_cI_b/l_b$ (where l_b is the full beam pin-to-pin span length minus the column depth). The yield moments are taken as the positive and negative beam yield moment strengths, computed considering the effective slab width per ACI 318-02. No strength degradation is specified, and pinching moments are assumed as one-fifth of the yielding moments, again based on experimental results.

Input parameters for the bond slip rotational spring are determined according to the formulation proposed by Morita and Kaku (1984), with some modifications. Fig. 16 illustrates the assumed stress and strain distributions of a longitudinal beam reinforcing bar (after yielding) in an interior joint. These and additional assumptions used to compute the moment vs. rotation relation of the bond slip spring can be summarized as follows:

(a) The tensile stress distribution in a longitudinal beam bar along the column depth is linear before yielding and bilinear after yielding (zero at the location where the bar begins to slip, and maximum at the beam/joint interface).

(b) The bond stress in the joint is uniformly distributed, and its magnitude is proportional to the reinforcing bar tensile strain at the beam/joint interface (ε_{st}).

(c) The amount of beam bar pullout slip at the beam/joint interface is computed by integrating beam bar strains from where bond slip starts to the interface. For interior joints, L_y (the length within which beam bar yielding occurs in the joint) is limited to the column depth, and the sum of L_s and L_y (the distance from where bond slip starts to the interface) is limited to L_{cs} (the column depth plus half the beam depth).

(d) Rotations are estimated by the amount of pullout slip divided by the distance between top and bottom beam bars, neglecting the push-in of reinforcing bars in compression.

(e) The moment-rotation curve of the bond slip spring is assumed bi-linear (two lines meeting at the point of beam reinforcement yielding), even though the post-yield part of the curve is actually nonlinear because the amount of pullout slip after yielding depends on the maximum-to-yield stress ratio.
(f) The pinching moments (M_g) for the bond slip spring are determined as a function of the length of the bond slip region (L_s). For most specimens, with column depth to beam bar diameter ratios greater than about 15, this resulted in no pinching of the bond slip spring. Strength degradation is not considered in the bond slip spring.

Modifying Morita and Kaku (1984), the yield moments of the bond slip spring are taken equal to the yield moments of the plastic hinge spring in this study; the stiffness of the bond slip spring is computed with beam reinforcement only.

5. Application of the proposed connection model

The validity of the developed connection model can be demonstrated by applying it to interior beam-column connections listed in Tables 1 and 2. For each connection, input parameters for all elements constituting the connection model were calculated using actual material properties and member details. In the analysis process, the column axial load imposed during the test (if any) was

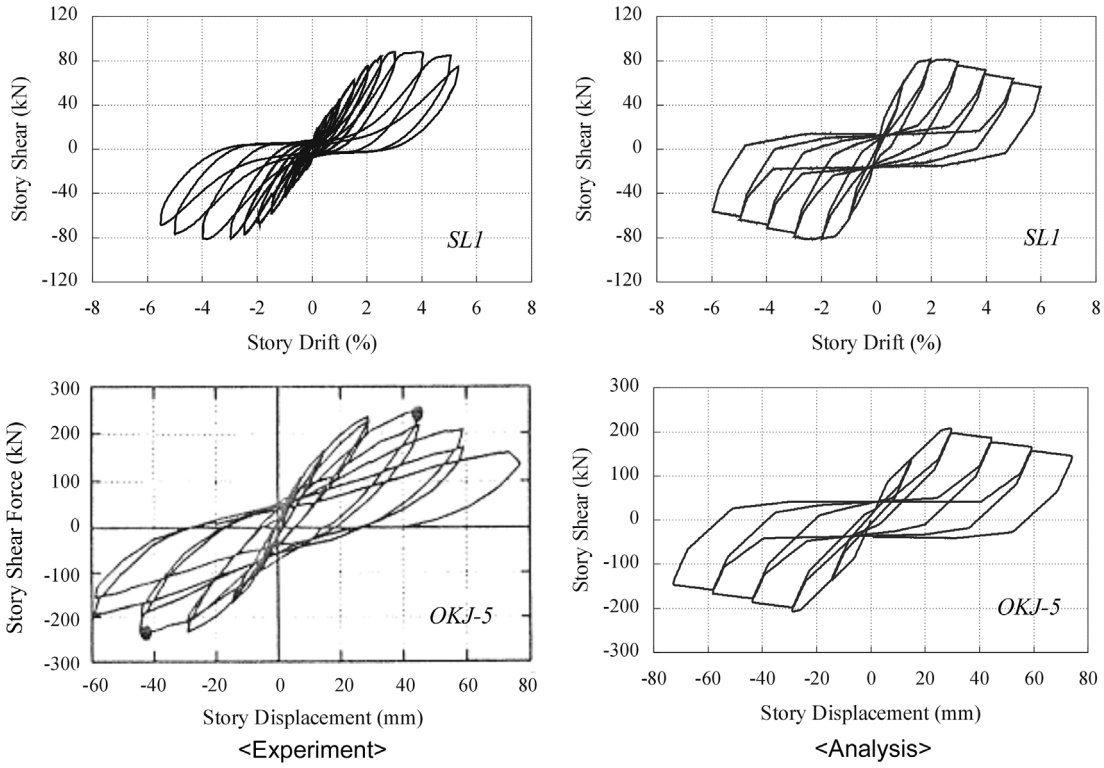

Fig. 17 Comparison of overall load-displacement responses from tests and analyses

applied first, followed by the lateral loading in a static manner.

As an example, Fig. 17 compares overall story shear vs. story drift response from the analyses and the experiments for specimens SL1 and OKJ-5. During the analyses, SL1 showed joint shear failure after beam hinging, and OKJ-5 underwent joint shear failure without beam hinging, as observed in the tests. Also, the connection model characterized well the strength decays occurring after joint shear failure. The maximum story shear force reached during the analysis of OKJ-5 was a bit smaller than the experimental one, because the analytical joint shear strength (from the MCFT) happened to be about 15% below the actual value. In both analyses, joint shear failure occurred slightly earlier than in the tests (in terms of story drift), in part because analytical joint shear strains at the point of joint shear strength were smaller than experimental ones.

In some test specimens that failed in a BJ-type mode, the developed connection model only showed either joint shear failure or beam hinging, in part because the joint and beam models (connected in series) typically have small post-yield stiffness. For instance, the joint shear response obtained from the analysis of specimen SL4 never got to the point of joint shear failure (up to 6% story drift), as the analytical joint shear strength was somewhat larger than the experimental joint shear stresses. However, even in this case analytical joint shear deformations contributed more than 20% to the overall story drift of the connection model, a feature that would have been lost without considering joint shear deformations in the model. In conclusion, then, the developed connection model was able to well represent the overall experimental load-displacement response of connection subassemblies, and it is therefore likely well-suited for use in RC frame analyses.

6. Conclusions

This study proposes an analytical method for estimating the hysteretic joint shear behavior of RC beam-column connections and develops a DRAIN-2DX connection model capable of explicitly incorporating this behavior into frame analysis. A summary of key findings and conclusions is as follows:

1. From investigating numerous beam-column connection tests, nonlinear hysteretic joint shear stress vs. strain behavior was characterized as a quad-linear envelope curve (connecting the points of joint shear cracking, reinforcement yielding, and joint shear strength) with a descending slope after failure and typical hysteretic properties.
2. An analytical scheme was utilized to estimate the nonlinear hysteretic shear stress vs. strain response of beam-column joints without testing. The envelope curve of joint shear response was computed using the MCFT, while the hysteretic properties were represented by an appropriate hysteresis model, calibrated based on experimental results. In general, the proposed analytical scheme gave good results in comparison with experiments.
3. A connection model was developed to explicitly incorporate nonlinear joint shear behavior into frame analysis. (The connection model also addressed fixed end rotations at beam/joint interfaces due to bond slip and yielding of longitudinal beam bars in the joint, as well as plastic hinge rotations near the ends of beams.) The connection model was able to well represent the overall cyclic load-displacement response of beam-column connection subassemblies, and to capture contributions from the beams, the columns, and the joint to overall story drift.

4. The developed connection model, along with the proposed analytical scheme for joint shear response, can further be used to evaluate global performance of RC frame structures, including estimates of local strength and ductility demands on constituent frame members. This connection model can be particularly effective in the analysis of frame structures where moderate to large joint shear deformations may occur.
5. The proposed analytical scheme employing the MCFT for estimating joint shear response does not address the potential effect of eccentricity between beam and column centerlines nor the presence of transverse beams (and/or floor slabs) on joint shear strength; these are topics open to future research.

References

ACI Committee 318 (2002), "Building code requirements for reinforced concrete (ACI 318-02) and commentary (ACI 318R-02)", American Concrete Institute, Farmington Hills, Michigan.

ACI-ASCE Committee 352 (2002), "Recommendations for design of beam-column connections in monolithic reinforced concrete structures (ACI 352R-02)", American Concrete Institute, Farmington Hills, Michigan.

Alath, S. and Kunnath, S. (1995), "Modeling inelastic shear deformation in RC beam-column joints", *Proc. Tenth Conf. on Engineering Mechanics*, University of Colorado at Boulder, Boulder, Colorado, 822-825.

Anderson, J.C. and Townsend, W.H. (1977), "Models for RC frames with degrading stiffness", *J. Struct. Div.*, ASCE, **103**(ST12), 1433-1449.

Biddah, A. and Ghobarah, A. (1999), "Modeling of shear deformation and bond slip in reinforced concrete joints", *Struct. Eng. Mech.*, **7**(4), 413-432.

Bonacci, J. and Pantazopoulou, S. (1993), "Parametric investigation of joint mechanics", *ACI Struct. J.*, **90**(1), 61-71.

CEB (1996), *RC Frames under Earthquake Loading*, Thomas Telford, London, UK, 303 pp.

Collins, M.P. and Mitchell, D. (1991), *Prestressed Concrete Structures*, Prentice Hall, Upper Saddle River, NJ, 766 pp.

Elmorsi, M., Kianoush, M.R. and Tso, W.K. (1998), "Lightly reinforced beam column joint model for frame analysis", *Sixth U.S. Nat. Conf. on Earthquake Engineering*, Seattle, Washington.

Filippou, F.C., D'Ambrisi, A. and Issa, A. (1999), "Effects of reinforcement slip on hysteretic behavior of reinforced concrete frame members", *ACI Struct. J.*, **96**(3), 327-335.

Fleury, F., Reynouard, J.M. and Merabet, O. (1999), "Finite element implementation of a steel-concrete bond law for non-linear analysis of beam-column joints subjected to earthquake type loading", *Struct. Eng. Mech.*, **7**(1), 35-52.

Foutch, D.A., Shi, S. and Yun, S.-Y. (2003), "Element 10: A stiffness and strength degrading element developed for the SAC steel program", Distributed with DRAIN-2DX by the National Information Service for Earthquake Engineering (NISEE), Available from http://nisee.berkeley.edu/software/drain2dx/.

Fujii, S. and Morita, H. (1991), "Comparison between interior and exterior RC beam-column joint behavior", *Design of Beam-Column Joints for Seismic Resistance (SP-123)*, American Concrete Institute, Detroit, Michigan, 145-165.

Giberson, M.F. (1969), "Two nonlinear beams with definitions of ductility", *J. Struct. Div.*, ASCE, **95**(ST2), 137-157.

Joh, O., Goto, Y. and Shibata, T. (1991), "Behavior of reinforced concrete beam-column joints with eccentricity", *Design of Beam-Column Joints for Seismic Resistance (SP-123)*, American Concrete Institute, Detroit, Michigan, 317-357.

Kitayama, K., Otani, S. and Aoyama, H. (1991), "Development of design criteria for RC interior beam-column joints", *Design of Beam-Column Joints for Seismic Resistance (SP-123)*, American Concrete Institute, Detroit, Michigan, 97-123.

Kitayama, K. (1992), "Restoring force characteristics in reinforced concrete beam-column joints", *Transactions of the Japan Concrete Institute*, **14**, 491-498.
Krawinkler, H. and Mohasseb, S. (1987), "Effects of panel zone deformations on seismic response", *J. of Construction Steel Research*, **8**, 233-250.
Krawinkler, H. (2001), "State of the art report on systems performance of steel moment frames subjected to earthquake ground shaking", FEMA-355C, Federal Emergency Management Agency, Washington, DC.
Kurose, Y., Guimaraes, G.N., Zuhua, L., Kreger, M.E. and Jirsa, J.O. (1991), "Evaluation of slab-beam-column connections subjected to bi-directional loading", *Design of Beam-Column Joints for Seismic Resistance (SP-123)*, American Concrete Institute, Detroit, Michigan, 39-67.
Leon, R.T. (1990), "Shear strength and hysteretic behavior of interior beam-column joints", *ACI Struct. J.*, **87**(1), 3-11.
Lowes, L.N. and Altoontash, A. (2002), "Modeling the response of RC building beam-column joints subjected to earthquake loading", *Seventh U.S. Nat. Conf. on Earthquake Engineering*, Boston, Massachusetts.
Meinheit, D.F. and Jirsa, J.O. (1981), "Shear strength of RC beam-column connections", *J. Struct. Div.*, ASCE, **107**(ST11), 2227-2244.
Morita, S. and Kaku, T. (1984), "Slippage of reinforcement in beam-column joint of reinforced concrete frame", *Eighth World Conf. on Earthquake Engineering*, San Francisco, CA, 477-484.
Noguchi, H. and Kashiwazaki, T. (1992), "Experimental studies on shear performances of RC interior column-beam joints with high-strength materials", *Tenth World Conf. on Earthquake Engineering*, Balkema, Rotterdam, 3163-3168.
Otani, S. (1974), "Inelastic analysis of RC frame structures", *J. Struct. Div.*, ASCE, **100**(ST7), 1433-1449.
Pantazopoulou, S.J. and Bonacci, J.F. (1994), "On earthquake-resistant reinforced concrete frame connections", *Canadian Journal of Civil Engineering*, **21**, 307-328.
Paulay, T. and Priestley, M.J.N. (1992), *Seismic Design of Reinforced Concrete and Masonry Buildings*, John Wiley & Sons, New York, NY, 744 pp.
Prakash, V., Powell, G.H. and Campbell, S. (1993), "DRAIN-2DX base program description and user guide", University of California, Berkeley, California.
Raffaelle, G.S. and Wight, J.K. (1992), "R/C eccentric beam-column connections subjected to earthquake-type loading", Research Report UMCEE 92-18, University of Michigan, Ann Arbor, Michigan.
Shin, M. and LaFave, J.M. (2004a), "Seismic performance of reinforced concrete eccentric beam-column connections with floor slabs", *ACI Struct. J.*, **101**(3), 403-412.
Shin, M. and LaFave, J.M. (2004b), "Reinforced concrete edge beam-column-slab connections subjected to earthquake loading", *Magazine of Concrete Research*, **56**(5), 273-291.
Stevens, N.J., Uzumeri, S.M. and Collins, M.P. (1991), "Reinforced concrete subjected to reversed cyclic shear – experiments and constitutive model", *ACI Struct. J.*, **88**(2), 135-146.
Takeda, T., Sozen, M.A. and Nielsen, N.N. (1970), "Reinforced concrete response to simulated earthquakes", *J. Struct. Div.*, ASCE, **96**(ST12), 2557-2573.
Teng, S. and Zhou, H. (2003), "Eccentric reinforced concrete beam-column joints subjected to cyclic loading", *ACI Struct. J.*, **100**(2), 139-148.
Teraoka, M. and Fujii, S. (2000), "Seismic damage and performance evaluation of R/C beam-column joints", *The Second U.S.-Japan Workshop on Performance-Based Engineering for Reinforced Concrete Building Structures*, Hokkaido, Japan, 379-390.
Vecchio, F.J. and Collins, M.P. (1986), "The modified compression field theory for reinforced concrete elements subjected to shear", *ACI Struct. J.*, **83**(2), 219-231.
Vecchio, F.J. and Collins, M.P. (1988), "Predicting the response of reinforced concrete beams subjected to shear using modified compression field theory", *ACI Struct. J.*, **85**(3), 258-268.
Watanabe, K., Abe, K., Murakawa, J. and Noguchi, H. (1988), "Strength and deformation of reinforced concrete interior beam-column joints", *Transactions of the Japan Concrete Institute*, **10**, 183-188.
Youssef, M. and Ghobarah, A. (2001), "Modeling of RC beam-column joints and structural walls", *J. Earthq. Eng.*, **5**(1), 93-111.